

SCIENTIFIC REPORTS



OPEN

Dynamic coupling of plasmonic resonators

Suyeon Lee & Q-Han Park

Received: 13 November 2015

Accepted: 04 February 2016

Published: 25 February 2016

We clarify the nature of dynamic coupling in plasmonic resonators and determine the dynamic coupling coefficient using a simple analytic model. We show that plasmonic resonators, such as subwavelength holes in a metal film which can be treated as bound charge oscillators, couple to each other through the retarded interaction of oscillating screened charges. Our dynamic coupling model offers, for the first time, a quantitative analytic description of the fundamental symmetric and anti-symmetric modes of coupled resonators which agrees with experimental results. Our model also reveals that plasmonic electromagnetically induced transparency arises in any coupled resonators of slightly unequal lengths, as confirmed by a rigorous numerical calculation and experiments.

Plasmonic nano resonators formed by various metallic nanostructures are at the core of plasmonics and metamaterial researches. Novel features arise when resonators are coupled to each other, including cases such as plasmonic dimers^{1–3}, plasmon induced transparency^{4–11}, directional optical antenna^{12–14} and high refractive index metamaterials^{15,16}. The interaction of localized plasmons in nanoparticle dimers has been explained in terms of a simple dipolar interaction¹⁷ or plasmon hybridization^{1,18}, the more general method. Though these approaches provide a reasonable description of coupled nanoparticles, they fail to accommodate the dynamical behaviour of coupled plasmonic resonators with accurate quantitative predictions, one of the most important open questions in plasmonics and metamaterial research. Recently, a single plasmonic resonator has been rigorously identified as a radiating dipole oscillator^{19,20}. A plasmonic resonator, for instance a half-wavelength rectangular hole in a metal film, can be identified as a bound charge oscillator, and, accordingly, the scattering of light by a resonator can be quantitatively described in terms of the scattering spectrum of a bound charge oscillator^{20,21}. This realisation raises the possibility of rigorously describing the interaction between plasmonic resonators in terms of bound charge oscillators.

In this Letter, we clarify the nature of dynamic coupling in plasmonic resonators by showing that plasmonic resonators couple to each other through the retarded interaction of bound charge oscillators. We determine the dynamic coupling of resonators explicitly from their retarded interaction and screened charges, allowing us to develop quantitative descriptions of the fundamental symmetric and anti-symmetric modes of coupled resonators in good agreement with actual experiments and exact numerical results. Importantly, our dynamically coupled oscillator model predicts the presence of the plasmonic electromagnetically induced transparency (EIT) in any coupled resonators of unequal lengths. Our model provides an analytic and for the first time quantitative description of EIT in plasmonic resonators. We show that the EIT of coupled oscillators arises from the destructive interference of two fundamental modes with distinct phase properties and that, as we confirm experimentally, the same feature arises in coupled plasmonic resonators. Our dynamic coupling approach is not restricted to the rectangular hole-type resonators considered in this paper. It can be readily applied to interacting plasmonic resonators in general and various building blocks of metamaterials.

Results

Oscillator picture of coupled resonators. We first recall that a single plasmonic resonator can be identified as a radiating bound charge dipole oscillator²⁰. Consider for example a narrow rectangular hole of size $a \times b$ in a thin metal film. When light is incident upon the rectangular hole with a polarization perpendicular to its long side, the total cross section of the free standing rectangular hole is given by the normalized energy flow through it,

$$\sigma_{\text{slot}} = S_z^{\text{norm}} \times ab \approx 3\pi c^2 \frac{T^2 \omega^4}{(\omega^2 - \omega_0^2)^2 + T^2 \omega^6}, \quad (1)$$

Department of Physics, Korea University, Seoul 136-701, Korea. Correspondence and requests for materials should be addressed to Q.H.P. (email: qpark@korea.ac.kr)

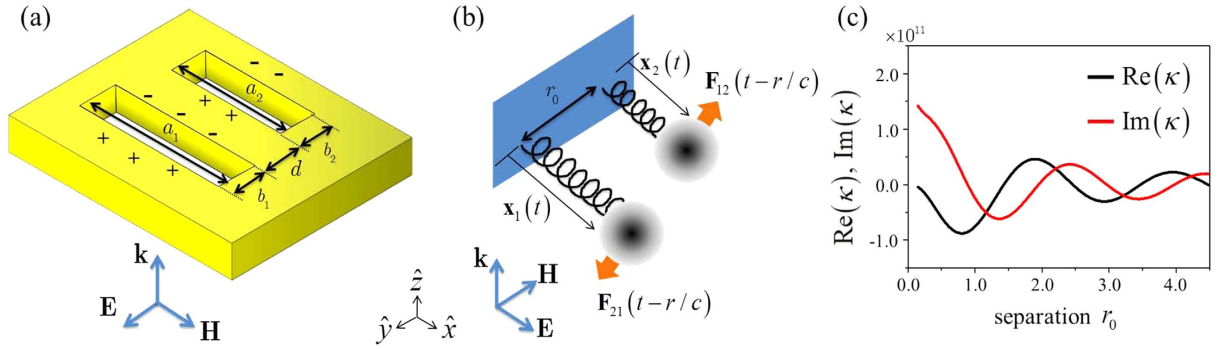


Figure 1. (a) Coupled slot resonators made of two rectangular holes of dimensions $a_1 \times b_1$ and $a_2 \times b_2$ separated by distance d in a perfect electric conductor (PEC) of negligible thickness. Light is incident normally upon the rectangular hole with a polarization perpendicular to its long side. (b) Bound charge oscillator model corresponding to coupled slot resonators. Bound charges, separated by distance r_0 at rest, oscillate along the x -direction only. (c) Dynamic coupling constant κ against charge separation.

where c is the speed of light, ω is the angular frequency of the incident wave and $\omega_0 = \pi c/a$. T is the dispersive time parameter,

$$T = \frac{16a}{3\pi^2 c} [\ln(b^2|\omega^2 - \omega_0^2|/4c^2) + 2\gamma - 3]^{-1}, \quad (2)$$

with the Euler's constant $\gamma (\approx 0.577)$. It was noted that a similar scattering property arises in a bound charge oscillator obeying the equation of motion,

$$m\ddot{x} = -m\omega_0^2 x + m\tau\ddot{x} + qE_0 e^{-i\omega t}, \quad (3)$$

where $x(t)$ is the displacement from the equilibrium position of a particle of mass m and charge q . Terms in the right side of Eq. (3) represent the restoring force, the radiative reaction force and the external force, respectively. The radiative reaction force, also known as the Abraham-Lorentz force, is responsible for the radiative energy loss characterized by the time constant $\tau (= q^2/6\pi\epsilon_0 mc^3)$. The total cross section of a bound charge oscillator σ_{osc} is defined as the ratio of the time-averaged radiated power to the incident intensity. Using the Larmor formula, $P = q^2 |\ddot{x}|^2/6\pi\epsilon_0 c^3$, we find

$$\sigma_{osc} = 6\pi c^2 \frac{\tau^2 \omega^4}{(\omega_0^2 - \omega^2)^2 + \tau^2 \omega^6}. \quad (4)$$

Comparing Eqs. (1) and (4) reveals that the scattering cross section is identical, after allowing for the 50% reduction in intensity for the slot case which represents only forward scattering. If we choose $\tau = T$, or equivalently introduce a dispersive oscillator mass,

$$m = \frac{\pi q^2}{32\epsilon_0 c^2 a} |\ln(b^2|\omega^2 - \omega_0^2|/4c^2) + 2\gamma - 3|. \quad (5)$$

Now, we consider two interacting plasmonic resonators, two rectangular holes of dimensions $a_1 \times b_1$ and $a_2 \times b_2$ separated by distance d as shown in Fig. 1a. Light is incident upon the holes with a polarization perpendicular to the long sides of the rectangles. The oscillator model of a plasmonic resonator suggests that an interaction between resonators can be treated as if it were an interaction between oscillating bound charges and we show that this is indeed the case. Since rectangular holes are complementary structures to rod type resonators, Babinet's principle indicates that the corresponding charged oscillators can be restricted to movement along the x -direction with displacements $\mathbf{x}_1(t) = x_1(t)\hat{x}$ and $\mathbf{x}_2(t) = x_2(t)\hat{x}$ as shown in Fig. 1b. The equations of motion for coupled oscillators are

$$\begin{aligned} m_1 \ddot{x}_1 &= -m_1 \omega_{10}^2 x_1 + m_1 \tau_1 \ddot{x}_1 + q_1 E_0 e^{-i\omega t + i\phi} + F_x^{21}, \\ m_2 \ddot{x}_2 &= -m_2 \omega_{20}^2 x_2 + m_2 \tau_2 \ddot{x}_2 + q_2 E_0 e^{-i\omega t} + F_x^{12}, \end{aligned} \quad (6)$$

where $\omega_{k0} = \pi c/a_k$ and a phase difference ϕ is allowed between the externally applied forces. The term F_x^{21} is the x -component of the Lorentz force \mathbf{F}_{21} acting on q_1 and likewise for F_x^{12} with $1 \leftrightarrow 2$,

$$\mathbf{F}_{21} = q_1^{sc} (\mathbf{E}_{21} + \dot{\mathbf{x}}_1 \times \mathbf{B}_{21}). \quad (7)$$

We include the effect of charge screening on the interaction of plasmonic resonators using a screened charge $q_1^{sc} = q_1 S$ with a screening factor S which will be determined later. \mathbf{E}_{21} and \mathbf{B}_{21} are the electric and magnetic fields due to charge q_2 measured at the retarded time $t-r/c$,

$$\begin{aligned} \mathbf{E}_{21} &= \frac{q_2^{sc}}{4\pi\epsilon_0} \left[\frac{\hat{\mathbf{r}} - \dot{\mathbf{x}}_2/c}{(1 - \dot{\mathbf{x}}_2 \cdot \hat{\mathbf{r}}/c)^3 r^2} + \frac{\hat{\mathbf{r}} \times \{(\hat{\mathbf{r}} - \dot{\mathbf{x}}_2/c) \times \ddot{\mathbf{x}}_2\}}{(1 - \dot{\mathbf{x}}_2 \cdot \hat{\mathbf{r}}/c)^3 r c^2} \right]_{ret}, \\ \mathbf{B}_{21} &= (\hat{\mathbf{r}}/c) \times \mathbf{E}_{21}, \end{aligned} \tag{8}$$

where $\mathbf{r} = \mathbf{r}_1 - \mathbf{r}_2 = r\hat{\mathbf{r}}$ with unit vector $\hat{\mathbf{r}}$ and \mathbf{r}_1 and \mathbf{r}_2 are the position vectors of the charges q_1 and q_2 respectively. We assume that displacements $x_1(t)$ and $x_2(t)$ are much smaller than separation d so that $\mathbf{r} \approx [d + (b_1 + b_2)/2]\hat{\mathbf{y}} \equiv r_0\hat{\mathbf{y}}$. This, together with the harmonic time dependence of x_2 with a factor $e^{-i\omega t}$, simplifies F_x^{21} to yield

$$F_x^{21} = -\frac{q_1^{sc} q_2^{sc}}{4\pi\epsilon_0} \left[\frac{\dot{x}_2(t - r_0/c)}{c r_0^2} + \frac{\ddot{x}_2(t - r_0/c)}{c^2 r_0} \right] \equiv q_1 q_2 \kappa x_2(t) \tag{9}$$

with the dynamic coupling coefficient

$$\kappa = \frac{S^2}{4\pi\epsilon_0} \left[\frac{i\omega}{c r_0^2} + \frac{\omega^2}{c^2 r_0} \right] e^{i\omega r_0/c}. \tag{10}$$

The time-averaged power provided by the external field to charge q_1 is

$$P_1 = \frac{1}{6\pi\epsilon_0 c^3} q_1^2 |\ddot{\mathbf{x}}_1|^2 - q_1 \text{Re}(\mathbf{E}_{21} \cdot \dot{\mathbf{x}}_1^*), \tag{11}$$

with the equivalent expression for power P_2 and charge q_2 also holding. Then the total cross section σ_c of the coupled oscillator, defined as the ratio of the total power $P_1 + P_2$ to the incident intensity, becomes

$$\sigma_c = \frac{q_1^2 |\ddot{\mathbf{x}}_1|^2 + q_2^2 |\ddot{\mathbf{x}}_2|^2}{6\pi\epsilon_0^2 c^4 E_0^2} - \frac{\text{Re}(q_1 \mathbf{E}_{21} \cdot \dot{\mathbf{x}}_1^* + q_2 \mathbf{E}_{12} \cdot \dot{\mathbf{x}}_2^*)}{\epsilon_0 c E_0^2}. \tag{12}$$

Determination of dynamic coupling. For a better understanding of coupling and charge screening, we consider the case of two identical oscillators with $m_1 = m_2 = m$ and $q_1 = q_2 = q$. Coupled identical oscillators admit two fundamental modes, symmetric and anti-symmetric. The symmetric mode is driven by external fields without a phase difference ($\phi = 0$) and is characterized by the steady state solution (see Supplementary Information for detailed derivation of Eq (13)–(17))

$$x_1^S = x_2^S = \frac{qE_0 e^{-i\omega t}/m}{\omega_0^2 - \omega^2 - i\tau\omega^3 - q^2\kappa/m}. \tag{13}$$

The corresponding total cross section becomes

$$\sigma_c^S = \frac{12\pi c^2 \tau^2 (\omega^4 + 6\pi\epsilon_0 c^3 \omega \kappa_I)}{(\omega_0^2 - \omega^2 - 6\pi\epsilon_0 c^3 \tau \kappa_R)^2 + \tau^2 (\omega^3 + 6\pi\epsilon_0 c^3 \kappa_I)^2}. \tag{14}$$

Similarly, the anti-symmetric mode is driven by external fields of phase difference $\phi = \pi$ and given by

$$x_1^A = -x_2^A = \frac{qE_0 e^{-i\omega t}/m}{\omega_0^2 - \omega^2 - i\tau\omega^3 + q^2\kappa/m}, \tag{15}$$

so that the corresponding total cross section becomes

$$\sigma_c^A = \frac{12\pi c^2 \tau^2 (\omega^4 - 6\pi\epsilon_0 c^3 \omega \kappa_I)}{(\omega_0^2 - \omega^2 + 6\pi\epsilon_0 c^3 \tau \kappa_R) + \tau^2 (\omega^3 - 6\pi\epsilon_0 c^3 \kappa_I)^2}. \tag{16}$$

Here, κ_R (κ_I) are the real (imaginary) part of the coupling coefficient κ in Eq. (10) which without the factor S^2 becomes singular as the separation r_0 between the two charges becomes zero. In the case of coupled plasmonic resonators of identical dimensions $a \times b$, as the separation between the two rectangular holes becomes zero, they merge into a single rectangular hole of size $a \times 2b$. Since the scattering cross section in (4), evaluated near the resonance $\omega \approx \omega_0$, is independent of the short side b , at the limit of zero separation we would expect the total scattering cross section of coupled identical resonators to reduce to that of a single resonator. It can be readily shown that this requirement is fulfilled with the choice of the screening factor $S = S_0$ where

$$S_0 \equiv 1 - \exp[-\sqrt{2/3} \omega r_0/c]. \tag{17}$$

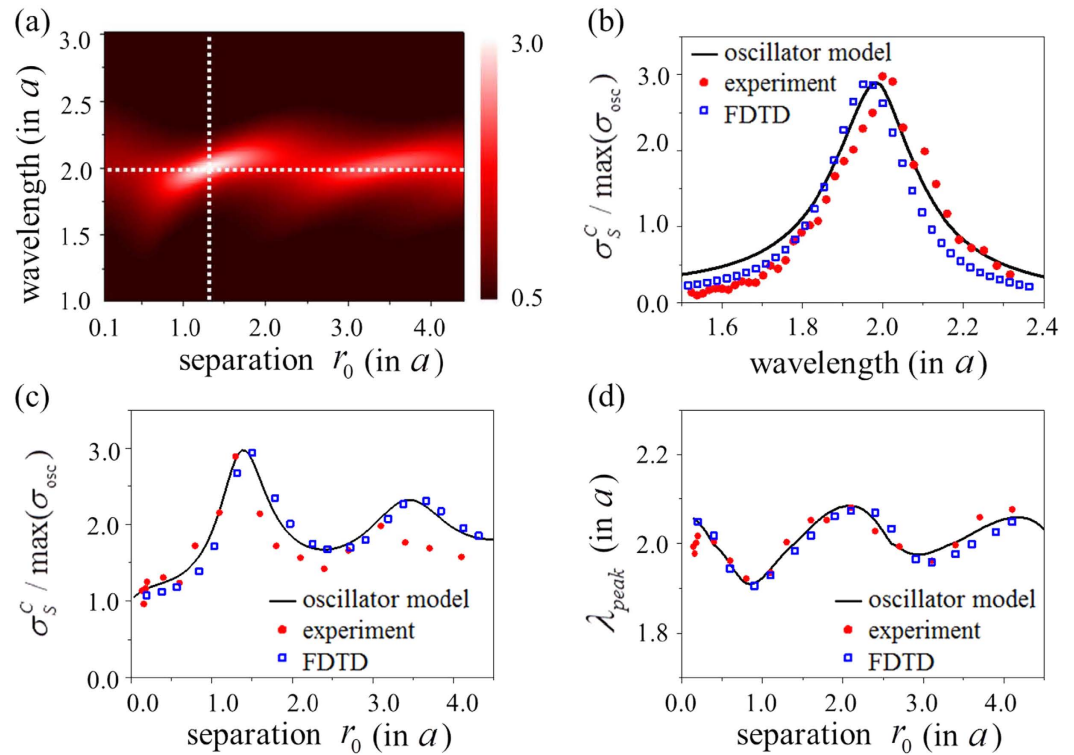


Figure 2. (a) Scattering cross section of the oscillator model in symmetric mode plotted against incident wavelength and charge separation. Scattering cross section is normalized by that of single resonator at the resonance, and wavelength and separation are in the unit of the long side of the rectangle a . (b) Vertical breaks of (a) from the oscillator model (thick line) in comparison with the experiment (thin line), and the FDTD calculation (square dot). Separations between oscillators are $1.3a$. (c) Horizontal break of (a) at resonance wavelength (black line) in comparison with the experiment (red dot), and the FDTD calculation (square dot). (d) Resonance peak shifts of the cross section in symmetric mode.

Finally, fixing the dynamic coupling coefficient in (10) with $S = S_0$ as shown in Fig. 1c, we establish the oscillator model for dynamically coupled resonators.

To confirm the validity of our model, we compare the total cross sections of coupled oscillators with numerically-calculated and experimentally-measured cross sections of corresponding coupled resonators. The results are shown in Fig. 2 in which the spectrum of the scattering cross section in symmetric mode given by (14) is plotted against resonator separation (the antisymmetric case is given in Supplementary Fig.S1). The scattering cross section is normalized by maximum value of the cross section from single resonator shown in Eq.(4). In Fig. 2b, the vertical breaks in the oscillator scattering cross section represent scattering spectra at the maximum scattering separation. The horizontal break shown in Fig. 2c at $\lambda = \lambda_0 = 2a$ (the black solid line) indicates that the cross section varies from 1 to 3 and converges to 2 in an oscillatory manner as the separation distance increases. This is in accordance with the expectation that the effect of coupling diminishes with larger separations. The positions of the spectral peaks in Fig. 2d show both blue and red shifts from the single resonator resonance, $\lambda = \lambda_0 = 2a$, depending on the degree of separation of the coupled resonators. Remarkably, all these properties predicted by the oscillator model turn out to be in excellent agreement with not only the scattering behaviour of coupled resonators calculated using a rigorous FDTD numerical method but also the experimental data from microwave measurement.

Plasmonic EIT in asymmetric resonators. One of the most intensively studied properties of coupled resonators is the plasmonic analogue of electromagnetically induced transparency (EIT) which arises from the interference between bright (symmetric) and dark (anti-symmetric) modes. Various coupled resonator systems such as the dipole-quadrupole antenna pair^{10,11} have been employed to demonstrate EIT but without analytic quantitative predictions. Here, we show that a simple system of two parallel rectangular holes of unequal size indeed leads to EIT by opening a dip in the scattering cross section. Our oscillator model approach presents an analytic expression for the scattering cross section which also shows reasonable quantitative agreement with experimental results. Consider the two non-identical rectangular holes specified in Fig. 1 where the aspect ratio $R = a_2/a_1$ is close to one. The steady state solution of the corresponding oscillator equation is given by (see Supplementary Information for derivation)

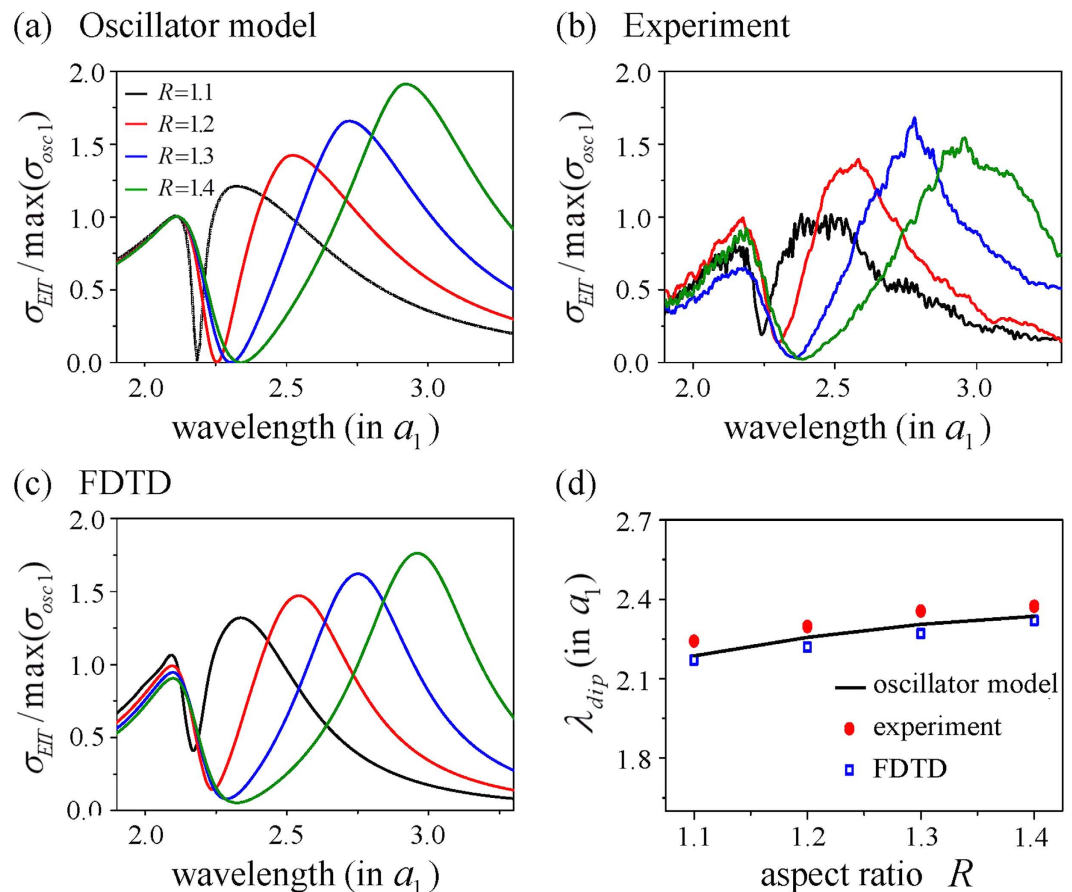


Figure 3. Plasmonic EIT in dynamically coupled resonators. Systems consist of two non-identical rectangular holes of dimensions $a_1 \times b_1$ and $a_2 \times b_2$ where the aspect ratio $R = a_2/a_1$ is chosen specifically with values $R=1.1$ (black), 1.2 (red), 1.3 (blue), and 1.4 (green) and $b_1 = b_2 = 0.1a_1$. (a) Scattering cross section spectra of corresponding oscillator models obtained from Eq. (19). (b) Microwave measurement of scattering cross sections of coupled resonators and (c) the FDTD numerical results. Scattering cross section is normalized by the cross section of resonant ($\omega = \omega_{10}$) single oscillator of dimension $a_1 \times b_1$ at the resonance, and wavelength is in the unit of a_1 . (d) Spectral dip positions against the aspect ratio obtained from the oscillator model (black line), the experiment (red circle), and the FDTD calculation (blue square).

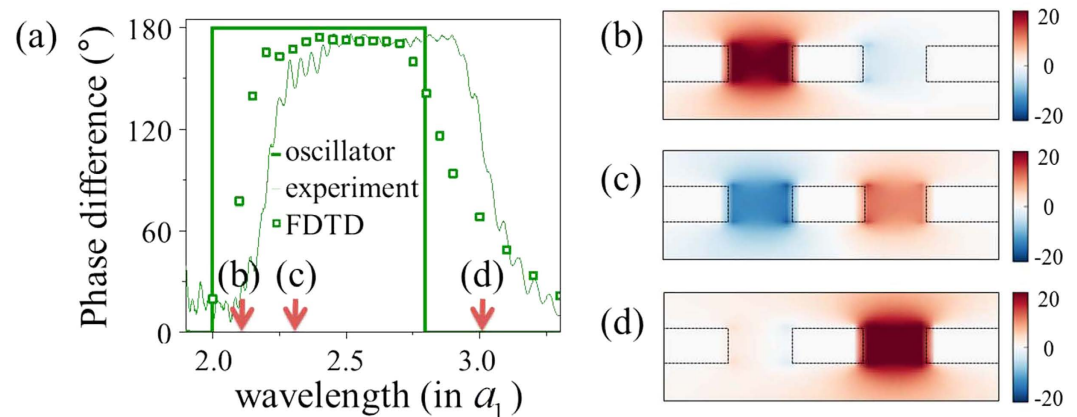


Figure 4. Properties of EIT modes. (a) Spectral phase differences in coupled resonators possessing the aspect ratio $R = 1.4$ and in the corresponding oscillator. The phase difference of the E_y -field component has been measured at the center of the two slots separated by distance $0.1a_1$ using a hairpin antenna (thin curve). This is compared with the FDTD result (square dot) and the phase difference in two bound charge oscillators (thick curve). (b–d) E_y field maps obtained by the FDTD calculation showing the excitation of the dark mode of EIT. Modes at (b) the first peak, (c) the dip and (d) the second peak of EIT spectrum.

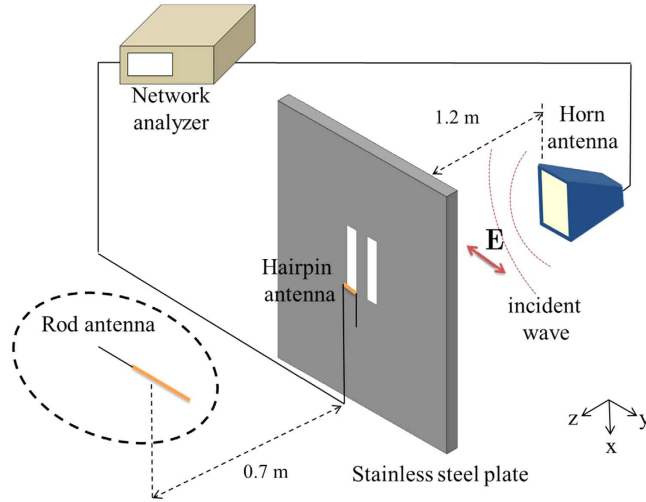


Figure 5. Experimental setup for measuring the microwave coupling of plasmonic resonators. We used the horn antenna as a source of y-polarized electric field, the rod antenna as a receiver for the far field detection, and the hairpin antenna for the near field detection.

$$\begin{aligned}
 x_1 &= \frac{q_1 (\Delta_2 + 6\pi\epsilon_0 c^3 \tau_2 \kappa) E_0 e^{-i\omega t}}{m_1 [\Delta_1 \Delta_2 - (6\pi\epsilon_0 c^3)^2 \tau_1 \tau_2 \kappa^2]}, \\
 x_2 &= \frac{q_2 (\Delta_1 + 6\pi\epsilon_0 c^3 \tau_1 \kappa) E_0 e^{-i\omega t}}{m_2 [\Delta_1 \Delta_2 - (6\pi\epsilon_0 c^3)^2 \tau_1 \tau_2 \kappa^2]} \\
 \Delta_k &\equiv \omega_{k0}^2 - \omega^2 - i\tau_k \omega^3, \quad \omega_{k0} = \frac{\pi c}{a_k}, \\
 \tau_k &= \frac{16a_k}{3\pi^2 c} \left| \ln(b_k^2 |\omega^2 - \omega_{k0}^2| / 4c^2) + 2\gamma - 3 \right|^{-1}; \quad k = 1, 2.
 \end{aligned} \tag{18}$$

The total scattering cross section is readily obtained from Eq. (12). In order to see the EIT behaviour explicitly, we note that the coupling constant can be approximated to $\kappa \approx i\omega^3 / 6\pi\epsilon_0 c^3$ if the separation of the rectangular holes is small. Then, the total scattering cross section simplifies to

$$\sigma_{EIT} \approx \frac{6\pi c^2 \omega^4 [\tau_1(\omega_{20}^2 - \omega^2) + \tau_2(\omega_{10}^2 - \omega^2)]^2}{|(\omega_{10}^2 - \omega^2 - i\tau_1 \omega^3)(\omega_{20}^2 - \omega^2 - i\tau_2 \omega^3) + \tau_1 \tau_2 \omega^6|^2}. \tag{19}$$

Note that $\sigma_{EIT}(\omega)$ possesses zero, $\sigma_{EIT}(\omega_{dip}) = 0$, at

$$\omega_{dip} \approx \left[\frac{\bar{\tau}_1 \omega_{20}^2 + \bar{\tau}_2 \omega_{10}^2}{\bar{\tau}_1 + \bar{\tau}_2} \right]^{1/2} \tag{20}$$

where we approximated $\tau_k(\omega)$ as $\bar{\tau}_k = \tau_k((\omega_{10} + \omega_{20})/2)$. This causes a dip in the broad resonance peak as shown in Fig. 3. Figure 3a shows the cross section spectrum in (19) while Fig. 3b,c show respectively the experimental and the FDTD numerical results for the scattering cross section of two rectangular holes corresponding to four different aspect ratios. Despite the simplicity, our oscillator model prediction manifesting EIT behaviour shows remarkable agreement with both the experimental and rigorous numerical results. Figure 3d compares the dip position predictions of the oscillator model with numerical and experimental results and once again the agreement is good since it is within 2 percent. Figure 4 describes the distinct spectral phase properties of EIT. We compared the phase differences between two oscillators with those between coupled resonators. To show phase difference between slots, we measure near-field of each slot using hairpin antenna. The E_y -field component has been measured near the edge of slots. The fields resonantly excited inside each of the rectangular holes correspond to the first and the second peaks in Fig. 4b,d. Around the transmission dip, both holes are excited and a π -phase difference is expected to arise due to the resonant excitation of a dark mode as shown in Fig 4c, a confirms that this is indeed the case.

Discussion

In conclusion, we have successfully described the behaviour of interacting plasmonic resonators with a coupled oscillator model which has been derived analytically from the full diffraction theory. The dynamic coupling coefficient of the oscillator model has been determined by the retarded interaction between oscillating screened

charges. The oscillator model allowed quantitative predictions about interacting resonators, particularly their EIT behaviour, which agreed with both numerical and experimental results. Our oscillator model approach is not restricted to rectangular-holed plasmonic resonators but can be readily applied to other types of plasmonic resonator such as rod-type nano antennae. Features of the bound charge oscillator model such as radiative damping, retarded interaction, and screening effects are also shared by coupled plasmonic resonators. This suggests that the dynamic coupling approach presented in this paper provides a general analytic framework for coupled resonators.

Methods

Microwave measurements have been performed using the experimental setup in Fig. 5. Slots are perforated on a stainless steel, which exhibits a nearly ideal metal behavior at micro-frequency of 2.6–3.9 GHz. A Hewlett-Packard 8719C network analyzer and a SGH260 standard gain horn antenna were used to generate the y-polarized electric field. To reduce the background noise, we surrounded the experimental setup using KSS-12 pyramidal absorbers. To measure the far and near components of electric field, we used a rod antenna made of a LMR-400 coaxial cable, and a hairpin antenna made of a RG-405 coaxial cable. Since the forward scattering amplitude is proportional to the total cross section according to the optical theorem, we have measured the forward scattering amplitude from a double slot and normalized it by the maximum value of the forward scattering amplitude from a single slot. To measure the phase difference between slots, we measured the near field component, using the hairpin antenna, near the edge of a slot in order not to disturb the field distribution.

We made numerical calculations using the FDTD (finite-difference time-domain) method where metal is assumed to be a perfect conductor which is valid in the microwave region. The grid size of the FDTD calculation was $0.025a \times 0.005a \times 0.0025a$.

References

- Nordlander, P., Oubre, C., Prodan, E., Li, K. & Stockman, M. I. Plasmon Hybridization in Nanoparticle Dimers. *Nano Lett.* **4**, 899–903 (2004).
- Aćimović, S. S., Kreuzer, M. P., González, M. U. & Quidant, R. Plasmon near-field coupling in metal dimers as a step toward single-molecule sensing. *ACS Nano* **3**, 1231–1237 (2009).
- Olk, P., Renger, J., Wenzel, M. T. & Eng, L. M. Distance dependent spectral tuning of two coupled metal nanoparticles. *Nano Lett.* **8**, 1174–8 (2008).
- Liu, N. *et al.* Planar Metamaterial Analogue of Electromagnetically Induced Transparency for Plasmonic Sensing. *Nano Lett.* **10**, 1103–7 (2010).
- Artar, A., Yanik, A. a. & Altug, H. Multispectral plasmon induced transparency in coupled meta-atoms. *Nano Lett.* **11**, 1685–9 (2011).
- Papasimakis, N. *et al.* Metamaterial with polarization and direction insensitive resonant transmission response mimicking electromagnetically induced transparency. *Appl. Phys. Lett.* **94**, 211902 (2009).
- Duan, X. *et al.* Polarization-insensitive and wide-angle plasmonically induced transparency by planar metamaterials. *Appl. Phys. Lett.* **101**, 143105 (2012).
- Ye, Z. *et al.* Mapping the near-field dynamics in plasmon-induced transparency. *Phys. Rev. B* **86**, 155148 (2012).
- Taubert, R., Hentschel, M., Kästel, J. & Giessen, H. Classical analog of electromagnetically induced absorption in plasmonics. *Nano Lett.* **12**, 1367–71 (2012).
- Liu, N. *et al.* Plasmonic analogue of electromagnetically induced transparency at the Drude damping limit. *Nat. Mater.* **8**, 758–62 (2009).
- Zhang, S., Genov, D. a., Wang, Y., Liu, M. & Zhang, X. Plasmon-Induced Transparency in Metamaterials. *Phys. Rev. Lett.* **101**, 047401 (2008).
- Simba, A. Y., Yamamoto, M., Nojima, T. & Itoh, K. Planar-type sectored antenna based on slot Yagi–Uda array. *IEE Proc. - Microwaves, Antennas Propag.* **152**, 347 (2005).
- Kosako, T., Kadoya, Y. & Hofmann, H. Directional control of light by a nano-optical Yagi–Uda antenna. *Nat. Photonics* **4**, 312–315 (2010).
- Kim, J. *et al.* Babinet-inverted optical Yagi–Uda antenna for unidirectional radiation to free space. *Nano Lett.* **14**, 3072–8 (2014).
- Choi, M. *et al.* A terahertz metamaterial with unnaturally high refractive index. *Nature* **470**, 369–373 (2011).
- Teguh Yudistira, H. *et al.* Fabrication of terahertz metamaterial with high refractive index using high-resolution electrohydrodynamic jet printing. *Appl. Phys. Lett.* **103**, 21106 (2013).
- Rechberger, W. *et al.* Optical properties of two interacting gold nanoparticles. *Opt. Commun.* **220**, 137–141 (2003).
- Prodan, E., Radloff, C., Halas, N. J. & Nordlander, P. A hybridization model for the plasmon response of complex nanostructures. *Science* **302**, 419–22 (2003).
- Kats, M. a., Yu, N., Genevet, P., Gaburro, Z. & Capasso, F. Effect of radiation damping on the spectral response of plasmonic components. *Opt. Express* **19**, 21748–53 (2011).
- Choe, J., Kang, J., Kim, D. & Park, Q. Slot antenna as a bound charge oscillator. *Opt. Express* **20**, 6521–6526 (2012).
- Kang, J., Choe, J., Kim, D. & Park, Q. Substrate effect on aperture resonances in a thin metal film. *Opt. Express* **17**, 15652–15658 (2009).

Acknowledgements

We thank Kyoung-Ho Kim for his help. This work was supported by Nano Material Technology Development Program (No. 2011-0020205) through the National Research Foundation of Korea (NRF), and the Center for Advanced Meta-Materials (CAMM-2014M3A6B3063710). Center for Advanced Meta-Materials was funded by the Ministry of Science, ICT and Future Planning as Global Frontier Project.

Author Contributions

Q.H.P. wrote the main manuscript text and S.Y.L. prepared Figures 1–5. All authors reviewed the manuscript.

Additional Information

Supplementary information accompanies this paper at <http://www.nature.com/srep>

Competing financial interests: The authors declare no competing financial interests.

How to cite this article: Lee, S. and Park, Q.-H. Dynamic coupling of plasmonic resonators. *Sci. Rep.* **6**, 21989; doi: 10.1038/srep21989 (2016).



This work is licensed under a Creative Commons Attribution 4.0 International License. The images or other third party material in this article are included in the article's Creative Commons license, unless indicated otherwise in the credit line; if the material is not included under the Creative Commons license, users will need to obtain permission from the license holder to reproduce the material. To view a copy of this license, visit <http://creativecommons.org/licenses/by/4.0/>